Progress In Electromagnetics Research, Vol. 124, 265–283, 2012

DETUNING STUDY OF IMPLANTABLE ANTENNAS INSIDE THE HUMAN BODY

N. Vidal[1, *], S. Curto[1], J. M. Lopez Villegas[1], J. Sieiro[1], and F. M. Ramos[1, 2]

[1]Radiofrequency Group, Electronics Department, University of Barcelona, Barcelona, Spain

[2]Francisco Albero S.A., Barcelona, Spain

Abstract—This study quantifies the detuning and impedance mismatch of antennas implanted inside the human body. Maximum frequency shifts caused by variations in the electrical properties of body tissues and different anatomical distributions were derived. The results are relevant to the design of implantable antennas. They indicate the bandwidth enhancement and initial tuning necessary for correct functioning. The study was carried out using electromagnetic modeling based on the finite-difference time-domain method and high-resolution anatomical models. Four anatomical computer models of two adults and two children were used. The implanted antennas operated in the Medical Implant Communication Service band. The most important detuning and impedance mismatch was found for subcutaneous locations and in areas where a layer of fat tissue was present. The maximum frequency shift towards higher frequencies was 70 MHz. The frequency shift did not occur symmetrically around 403 MHz, but was shifted towards higher frequencies.

1. INTRODUCTION

The number of microsystems designed to be implanted into the human body has increased in recent years [1]. A wide variety of sensors, microelectrodes, drug delivery devices, micro-machined transducers, micro actuators, surgical tools, etc. have been proposed. Some devices may need a wireless communication system and the communication link is a major challenge. The design of the antennas for biotelemetry

Received 5 December 2011, Accepted 13 January 2012, Scheduled 22 January 2012

* Corresponding author: Neus Vidal (nvidal@ub.edu).

applications is therefore currently of great interest. One of the challenges of the antenna design is possible detuning and impedance mismatch. Detuning effects have already been identified as a major challenge for the design of implantable antennas [2, 3]. The anatomical distribution as well as the different electrical properties and dimensions of the various tissues may affect the performance of the devices. Moreover, these anatomical characteristics vary from individual to individual. An antenna optimized for one location and person may not be adequately tuned for another location or person [2–4].

In recent years, much work has been performed on the design and characterization of implantable antennas [2–17]. In general, the design of the antennas takes into consideration specific single tissues and they are tested using tissue-equivalent liquids [3–10], mimicking gels [11, 12] and animals [13]. To date, detuning analysis has been limited to evaluating the resonance response of the proposed antennas implanted in fluids that simulate single biological tissues [14, 15]. Inside the human body, whether the design works or not may depend on detuning and impedance mismatch. The distribution of various body tissues may alter the performance of implanted antennas. Miniature broadband antennas may be required [14, 15, 18, 19].

The research reported here analyzes the detuning of implantable antennas when introduced into four anatomical whole-body human models. The main objective was to quantify the frequency shift and impedance mismatch and propose the bandwidth necessary for proper performance of implantable devices. We account not only for different tissues distributions, but also for different anatomical scenarios.

Electromagnetic modeling based on the finite-difference time-domain method (FDTD) was used. Four anatomical computer models of two adults and two children were used for the study. The models are referred to as the Virtual Family [20]. The implanted antennas were designed to operate in the 402–405 MHz frequency band approved by the Federal Communications Commission (FCC) for Medical Implant Communication Services (MISC) [21, 22]. For each of the human models, thirty different locations were analyzed. The locations were chosen taking into consideration an overview of implantable systems [1] as well as specific recently proposed medical devices [23–31].

The paper is organized as follows: Section 2 presents the method and simulation setup. In Section 3, the analysis in the adult male model is presented and discussed. The results are compared with those obtained for the female and children. A summary and the conclusions are presented in Section 4.

2. METHOD AND SIMULATION SETUP

This study is based on electromagnetic modeling using the FDTD method. Since its introduction by Yee in 1966 [32], this method has been used to solve Maxwell's differential equations in spatial grids in a wide range of application fields. Sullivan et al. [33] showed the capacity of the FDTD method to compute electromagnetic energy absorption in human tissues. The commercially available electromagnetic simulator SEMCAD — from Schmid & Partner Engineering AG. [34] was used.

PIFA antennas have been proposed for implantable medical devices [3–15]. Spiral-type radiators are usually applied to reduce the total antenna size. They are embedded inside dielectric substrates in order to avoid contact between the metal and the tissues, besides it leads to a lower absorbed power inside the human body [6]. Microstrip type antennas were also proposed and they showed similar performance despite lower radiation efficiency [5].

Two planar inverted-F antennas (PIFAs) were designed to be implanted inside the body. They resonate at the MISC frequency (403 MHz) in head and body tissues, i.e., one of the antennas was located inside liquid simulating mean head tissue and other was located inside liquid simulating mean body tissue. The dielectric parameters of the mean head and mean body tissues are shown in Table 1. They are in agreement with the FCC guidelines for human exposure to radiofrequency electromagnetic fields [35]. Figure 1 shows the planar geometry and cross-section of the proposed antenna. The antenna consists of three stacked layers with an embedded radiator. The ground plane is located at the bottom of the first layer. The radiator is printed at the bottom side of the second and third layer. It is a folded square inverted F structure that is shaped to fix in the interior perimeter

Table 1. Dielectric parameters of body tissues.

Tissue	ε_r	σ (S/m)	**Tissue**	ε_r	σ (S/m)
Mean-head tissue	43.5	0.87	Fat	11.62	0.08
Mean-body tissue	56.7	0.94	Kidney	66.32	1.09
Bone	13.14	0.09	Liver	51.18	0.65
Brain-grey-matter	57.37	0.74	Lung	23.79	0.37
Brain-white-matter	42.03	0.44	Muscle	57.10	0.79
Cerebellum	55.91	1.03	Skin	46.72	0.69
Cerebrospinal fluid	70.96	2.25	Skull/Vertebrae	13.14	0.09
Eye lens	37.48	0.37	Stomach	67.46	1.00

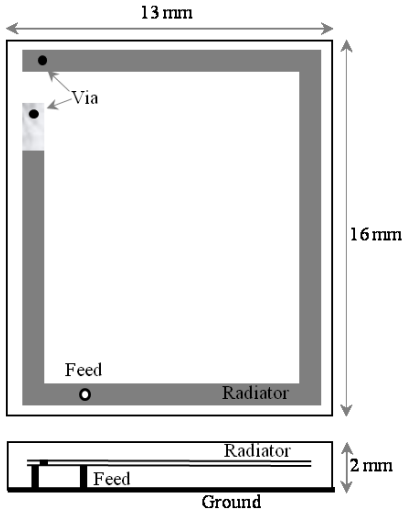

Figure 1. Planar geometry (top) and cross-section (bottom) of the proposed antenna.

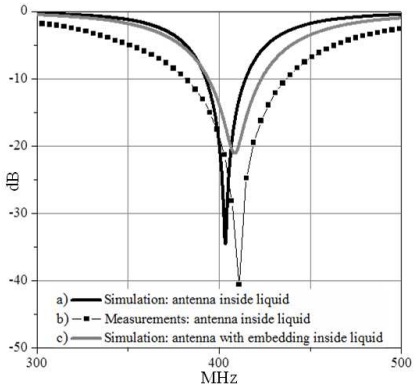

Figure 2. Simulated and measured return losses of the antenna design.

of the antenna module. A $50\,\Omega$ feed port excites the lower side of the radiator. The final antenna size is $13 \times 16 \times 2\,\text{mm}$ using LTCC dielectric substrate ($\varepsilon_r = 6.7$, $\sigma = 0.0026\,\text{S/m}$). LTCC has been tested for biocompatibility and it has already been used in different biological applications [36, 37]. The antenna geometry, with the main radiator positioned at the periphery, provides a wide internal space for future embedding of electronic integrated circuits. Different geometries were tested before choosing the proposed antenna; variations in the antenna bandwidth were observed however the detuning behavior was the same.

To validate the design, the antenna was fabricated and tested inside liquid simulating mean body tissue. The liquid was developed by mixing de-ionized water, sugar, salt and hydroxyethyl cellulose, in agreement with the FCC guidelines. Figure 2 shows a good agreement between simulated and measured antenna return losses inside the liquid that simulates mean body tissue. In this analysis only the implantable antenna has been considered. The detuning effect could be underestimated for implantable antennas without the whole transmitter set. Additional modeling was performed to analyze the influence of future integrated circuit embedded into the substrate. A metal box of different sizes was allocated inside the design and its influence in the return losses was analyzed. Figure 2(c)

Table 2. Characteristics of the four anatomical models taken from Christ et al. [20].

Age (years)	Sex	Height (m)	Mass (kg)	BMI (kg· m^{-2})
34	Male	1.74	70	23.1
26	Female	1.60	58	22.7
11	Female	1.46	36	16.7
6	Male	1.17	20	14.2

shows the antenna return loss with one of the analyzed metal boxes (10 mm × 10 mm × 0.5 mm). The main observed effect was impedance mismatching and small frequency shifts for the case of the antenna with the embedded metal box.

To perform the detuning analysis, the antennas (without the embedded metal box) were inserted into whole-body anatomical models. Four anatomical computer models of an adult male, an adult female and two children were used for the study. The main characteristics of the four models are shown in Table 2 and are taken from Christ et al. [20]. The models are based on high-resolution magnetic resonance (MR) images of healthy volunteers. All tissues and organs were reconstructed as three-dimensional (3D) unstructured triangulated surface objects, yielding high-precision images of individual features of the body.

The dielectric properties of the tissues were taken from the SEMCAD dataset. The anatomical models have more than 80 different tissue types; however, only the most representative cited in this paper are included in Table 1. Thirty different locations were analyzed: 5 inside the head and 25 over the trunk and limbs. Figure 3 shows side and front views of the adult male model with the locations studied. For some anatomical areas (arm, chest and abdomen) several locations were considered.

3. RESULTS AND DISCUSSION

Overall numerical results for the 4 models are presented in Tables 3 (adults) and 4 (children). Detuning and impedance mismatch can be observed for each implant location. In the next sub-section, the results for the adult male are presented. Then, in the subsection after that, those results are compared with those obtained for the adult female and the girl and boy. For comparison purposes we have fixed the plot scales for all the figures from 300 MHz to 500 MHz and from 0 to −50 dB.

Table 3. Simulated resonance frequency of the antennas inside the anatomical models of the adult male and female.

	ADULT MALE				ADULT FEMALE			
Locations	**Resonant Frequency (MHz)**	**Return Loss (dB)**	**-10 dB Bandwidth (MHz)**		**Resonant Frequency (MHz)**	**Return Loss (dB)**	**-10 dB Bandwidth (MHz)**	
Ref_head	403.0	-26.0	392.6-421.4	28.8	403.0	-26.0	392.6-421.4	28.8
Intracranial	382.1	-20.6	370.2-395.0	24.8	391.2	-21.07	378.2-403.8	25.6
Intracerebral	402.6	-24.5	391.8-413.4	21.6	406.5	-21.75	395.8-417.4	21.6
Eye	426.4	-16.8	415.8-436.6	20.8	431.5	-15.4	422.2-440.6	18.4
Ear	448.4	-22.4	435.8-460.6	24.8	435.2	-13.0	427.8-442.2	14.4
Glioma	408.5	-20.6	395.8-421.4	25.6	417.5	-29.8	405.4-429.4	24.0
Ref_body	403.0	-34.5	391.0-415.8	24.8	403.0	-34.5	391.0-415.8	24.8
Lung	430.4	-18.9	418.2-443.0	24.8	427.9	-22.5	415.8-440.6	24.8
Kidney	398.8	-15.9	385.4-407.0	21.6	397.2	-24.2	386.2-407.8	21.6
Liver	406.8	-27.1	395.8-418.2	22.4	405.4	-67.9	395.0-416.6	21.6
Stomach	401.9	-31.9	391.0-412.6	21.6	401.6	-32.4	391.0-412.6	21.6
Arm-1 (sub)	427.9	-42.2	415.8-439.8	24.0	445.3	-12.5	439.0-451.8	12.8
Arm-2	440.3	-18.1	429.4-451.0	21.6	451.6	-10.8	447.8-455.8	8.0
Arm-3	410.4	-32.5	400.6-419.8	19.2	445.3	-12.7	439.0-451.8	12.8
Arm-4	408.8	-28.7	397.4-420.6	23.2	408.4	-54.0	398.2-419.0	20.8
Chest-1	440.4	-17.5	431.0-450.2	19.2	443.0	-12.7	436.6-449.4	12.8
Chest -2	446.0	-12.2	439.8-451.8	12	457.1	-8.5	---	---
Chest -3	450.1	-11.9	444.6-455.8	11.2	468.3	-6.8	---	---
Chest -4	431.0	-16.1	422.2-439.8	17.6	473.9	-6.0	---	---
Chest -5	406.8	-35.2	396.6-417.0	20.4	479.9	-5.9	---	---
Chest -6	405.4	-29.4	394.2-416.6	22.4	473.6	-6.0	---	---
Chest_7	421.3	-20.2	410.2-432.6	22.4	403.6	-49.4	392.6-414.2	21.6
Abdomen-1	431.0	-22.4	421.4-440.6	19.2	435.5	-13.6	428.6-443.0	14.4
Abdomen-2	444.7	-16.6	435.8-454.2	18.4	453.2	-9.7	---	---
Abdomen-3	424.2	-23.0	413.4-435.0	21.6	442.7	-13.3	435.8-450.2	14.4
Abdomen-4	406.6	-42.5	397.4-415.8	18.4	401.2	-23.5	390.2-412.9	22.7
Abdomen-5	406.4	-46.7	397.4-415.8	18.4	395.2	-18.3	384.6-406.2	21.6
Wrist (sub)	439.6	-19.4	430.2-449.4	19.2	445.5	-13.2	438.2-452.6	14.4
Hip	404.3	-27.0	392.6-415.8	23.2	403.2	-35.7	393.0-413.4	20.4
Leg	413.0	-38.7	403.8-423.0	19.2	453.4	-9.7	---	---
Knee-1	422.2	-33.9	411.8-432.6	20.8	449.0	-11.8	443.8-454.2	10.4
Knee-2	408.6	-33.4	398.2-419.0	20.8	453.3	-9.8	---	---

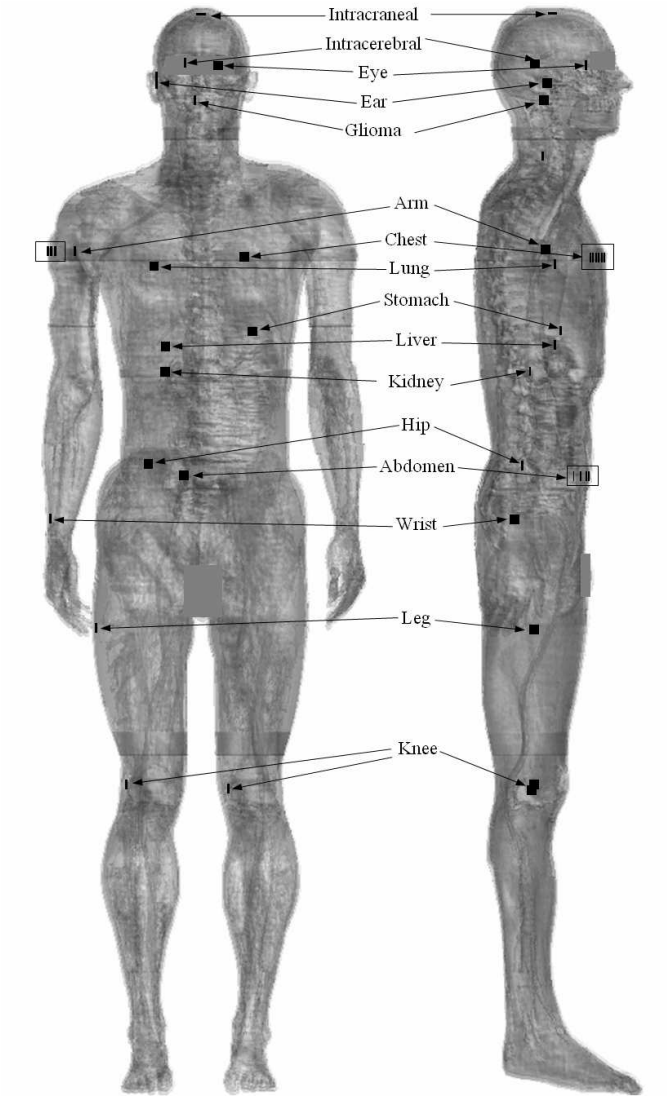

Figure 3. Front and side view of the adult male anatomical model with the locations where the antenna was implanted. For some anatomical areas (arm, chest and abdomen) several locations were considered and this is indicated by a black rectangle.

3.1. Results for the Male Model

When the antenna was located inside the head, a maximum detuning towards higher frequencies of 45.4 MHz was observed (Table 3) respect

Table 4. Simulated resonance frequency of the antennas inside the anatomical models of the children.

	GIRL				BOY			
Locations	**Resonant Frequency (MHz)**	**Return Loss (dB)**	**-10 dB Bandwidth (MHz)**		**Resonant Frequency (MHz)**	**Return Loss (dB)**	**-10 dB Bandwidth (MHz)**	
Ref_head	403.0	-26.0	392.6-421.4	28.8	403.0	-26.0	392.6-421.4	28.8
Intracranial	396.5	-30.1	-384.6-408.6	24.0	395.5	-28.4	383.0-408.6	25.6
Intracerebral	402.6	-24.6	391.8-413.4	21.6	404.0	-25.8	392.6-415.8	23.2
Eye	428.0	-16.1	418.2-437.4	19.2	437.6	-12.7	430.2-444.6	14.4
Ear	415.5	-23.3	404.6-427.0	22.4	428.5	-16.7	419.0-428.2	19.2
Glioma	405.1	-29.8	392.6-417.4	24.8	404.6	-43.8	392.8-417.4	25.6
Ref_body	403.0	-34.5	391.0-415.8	24.8	403.0	-34.5	391.0-415.8	24.8
Lung	428.8	-21.4	417.4-440.6	23.2	427.7	-21.4	415.8-439.8	24
Kidney	396.7	-23.4	386.2-407.8	11.6	396.0	-22.4	385.4-407.0	21.6
Liver	405.9	-44.9	395.8-416.6	20.8	404.6	-33.0	394.2-415.0	20.8
Stomach	402.8	-29.7	392.6-413.4	20.8	400.7	-27.9	390.2-411.8	21.6
Arm-1 (sub)	431.3	-26.4	421.4-441.4	20.0	435.5	-21.7	425.4-445.4	20
Arm-2	427.7	-28.5	417.4-438.2	20.8	444.9	-16.6	435.8-453.4	17.6
Arm-3	404.5	-29.2	394.2-415.0	20.8	409.5	-45.5	399.0-419.8	20.8
Arm-4	406.2	-30.0	395.8-416.6	20.8	407.0	-34.0	396.6-417.4	20.8
Chest-1	426.5	-26.2	415.8-437.4	21.6	422.0	-19.5	423.0-443.0	20.0
Abdomen-1	436.2	-18.5	427.0-445.4	18.4	437.2	-16.7	428.6-446.2	17.6
Abdomen-2	416.3	-28.7	406.2-427.0	20.8	418.2	-24.4	408.6-428.6	20
Wrist (sub)	421.6	-25.8	411.0-431.8	20.8	441.2	-17.4	432.6-450.2	17.6
Hip	411.9	-49.1	401.4-422.2	20.8	405.5	-34.2	395.0-416.6	21.6
Leg	452.1	-12.0	447.0-457.4	10.4	446.6	-14.1	439.0-454.2	15.2
Knee-1	435.5	-20.7	425.4-445.4	20.0	443.5	-15.1	435.0-451.8	16.8
Knee-2	447.8	-15.1	439.8-455.8	16.0	438.8	-17.5	429.4-447.8	18.4

the MISC reference frequency. The maximum detuning towards lower frequencies was 20.9 MHz. Figure 4 shows the simulated return losses (S_{11}) at different head locations. Different labels have been used for each curve to differentiate the curves inside each figure. The maximum detuning towards higher frequencies was found at the ear location and it could be attributed to the proximity of the skull, mandible and eye lens, which have lower dielectric parameters than the mean head tissue. The maximum detuning towards lower frequencies was observed to occur for the intracraneal location and must be attributed to the high dielectric parameters of the cerebrospinal fluid (Table 1).

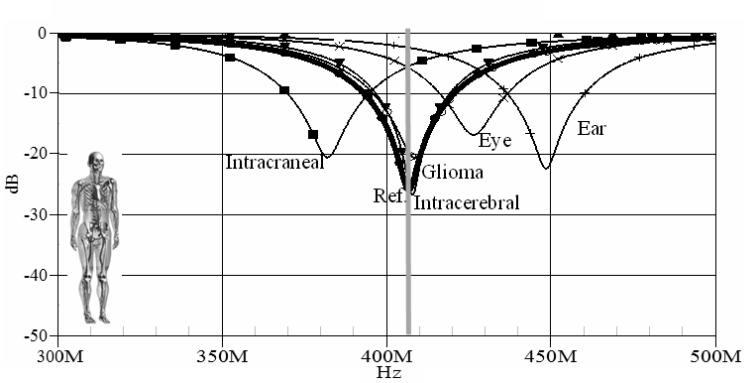

Figure 4. Simulated return losses for the implanted antenna inside the head of the male anatomical computer model. The gray vertical line corresponds to the MISC reference frequency. The thick black line corresponds to the response of the liquid simulating the head reference tissue.

It is important to note that the frequency shift was observed to occur in a fashion that was not symmetrically around 403 MHz. For 4 of the 5 locations studied, the resonant frequency shifted above the MISC band. On average, the resonant frequency shifted 13.15 MHz above the MISC band. From the analysis of the head, the maximum observed mismatch deviation from the reference was about 10.1 dB. For all the cases studied, the resonance return losses remained below −10 dB (Table 3).

Results from inside the trunk and limbs vary greatly depending on where the antenna was positioned. Inside the organs, the observed frequency shift is related to the dielectric parameters of the specific tissue. The lung tissue, with the smallest dielectric constant values (Table 1), produces the highest detuning of 27.4 MHz towards higher frequencies. Organs like the kidney, which has one of the highest dielectric constant values, yielded a maximum frequency shift towards lower frequencies of −4.2 MHz. In the hip area, small detuning values were also obtained (Table 3).

When the antenna was positioned at subcutaneous locations, the detuning was always found to shift towards higher frequencies (Table 3). This could be attributed to the presence of a fat layer with a low dielectric constant and also to the proximity of the skin-air interface. The antenna was placed 2 to 4 mm inside the skin-air interface. The specific depth depends on the curvature of the specific anatomical locations. In curved areas, it was necessary to place the antenna deeper (4 mm) than in flat zones. Results from some of

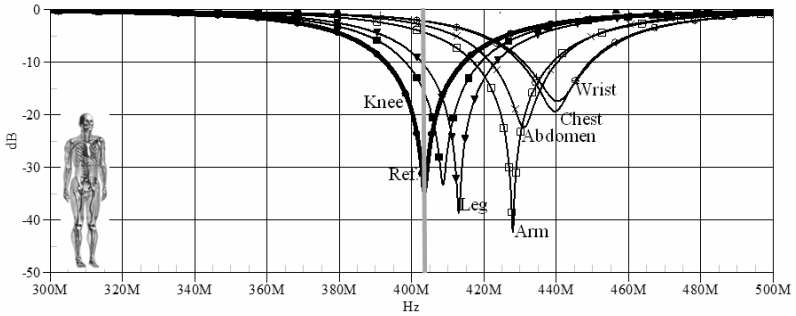

Figure 5. Simulated return losses for the implanted antenna located in several subcutaneous positions inside the male anatomical computer model (Figure 3). The gray vertical line corresponds to the MISC reference frequency. The thick black line corresponds to the response of the liquid simulating the body reference tissue.

the subcutaneous locations considered in the study (abdomen, arm, chest, knee, leg, wrist) are presented in Figure 5. The arm, chest and abdominal zones produced the greatest detuning of the antenna. This can mainly be attributed to the presence of a fat layer. Due to the flatness of the wrist, the antenna could be positioned very close to the skin-air interface (2 mm) and a shift towards a higher frequency was also obtained.

The antenna locations inside the arm, chest and abdominal regions were specifically analyzed to study the influence of fat tissue. Several positions, from 2 to 40 mm from the skin-air interface, were considered (Figure 6). The behavior was the same for the 3 regions and maximum detuning was derived (Table 3).

At the arm zone (Figure 6(a)) it can be seen that the resonant frequency at the subcutaneous location (location 1) increased when the antenna was located deeper inside the arm; this is attributed to the presence of a fat layer. Once the antenna was located inside the muscle tissue, the detuning was almost negligible because the dielectric properties of muscle tissue are very similar to those of mean body tissue. Results from inside the chest and abdominal regions show the same behavior (Figures 6(b), (c)). Maximum frequency shift values were obtained inside the chest and were the greatest obtained from the whole of the male body. Maximum detuning of 47.1 MHz was observed.

It is important to highlight that overall results from inside the trunk and limbs show similar behavior to that inside the head. For

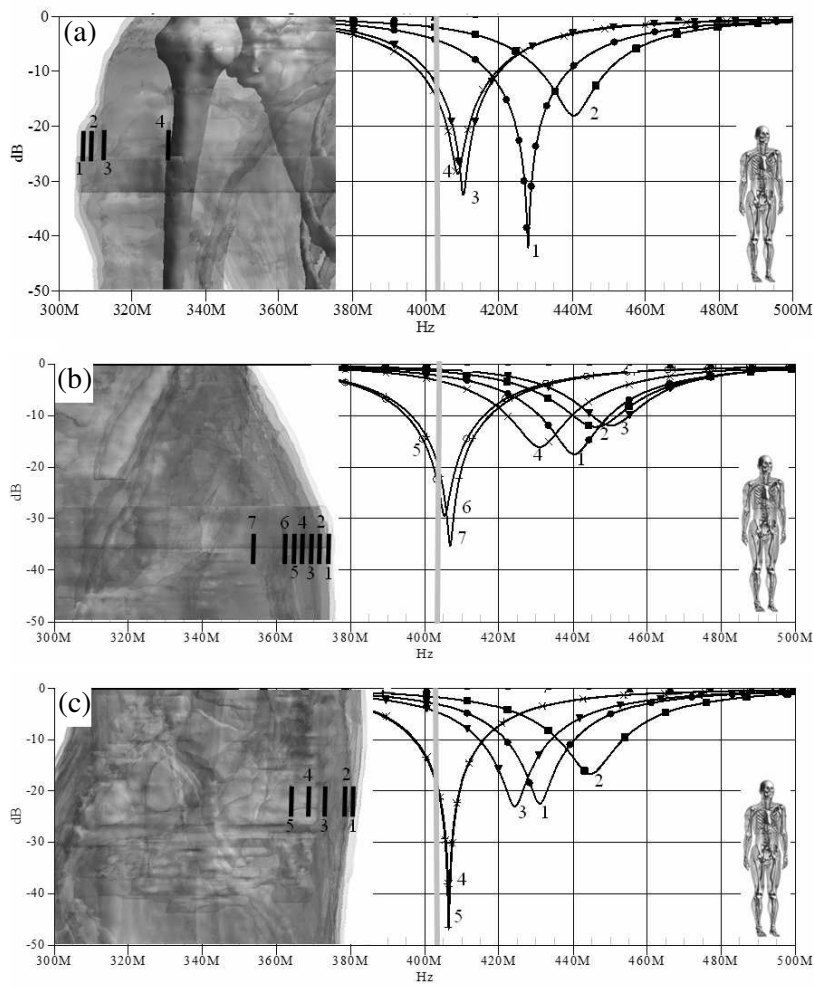

Figure 6. Simulated return losses for the antenna implanted inside (a) the arm, (b) the chest and (c) the abdomen of the male anatomical computer model. The gray vertical line corresponds to the MISC reference frequency. Inside (a) the arm the antenna was located 2 mm (1), 6 mm (2), 15 mm (3) from the air-skin interface and next to the bone (4). In (b) the chest area the antenna was positioned 4 mm (1), 8 mm (2), 12 mm (3), 16 mm (4), 20 mm (5), 24 mm (6) and 40 mm (7) from the air-skin interface. Finally, inside (c) the abdomen the antenna was positioned 4 mm (1), 8 mm (2), 20 mm (3), 30 mm (4) and 40 mm (5) from the air-skin interface.

28 of the 30 locations studied, the resonant frequency shifted above the MISC band (Table 3). This contrasts with previous studies that calculated the detuning response considering single simulating liquids [14, 15].

In the case of the trunk and limbs, the maximum mismatch deviation observed for the reference was 22.6 dB, which was higher than for the head. For all the cases studied, the resonance return losses remained below −10 dB. The highest mismatch occurred in the chest area (Table 3).

3.2. Results from the Anatomical Female and Kids Models

In this section we analyze the influence of the anatomical differences between models of different people on antenna detuning. The antenna was located inside the anatomical computer models of the adult female, the boy and the girl. The locations presented in Figure 3 were considered and the same systematic analysis presented in the previous subsection for the male case was performed. Due to the thinner anatomical tissue layers, for the analysis of the chest and the abdominal areas of the children, some specific locations were not considered. The overall numerical results from the adult female and the girl/boy are presented in Tables 3 and 4 respectively.

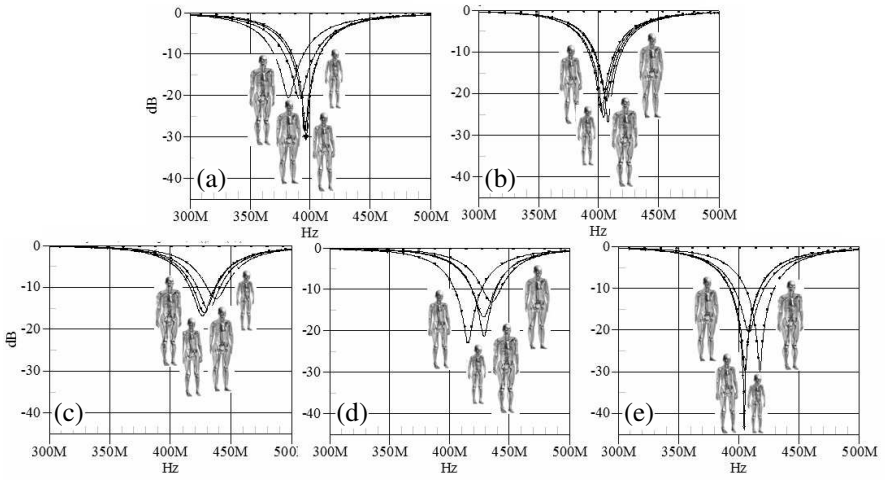

Figure 7. Simulated return losses for the antenna implanted inside the head for the four anatomical computer models. Results for (a) intracranial, (b) intracerebral, (c) ear, (d) eye and (e) glioma regions are presented.

Figure 7 shows the simulated return losses for the four body models when the antenna was located inside the head, at the intracranial, intracerebral, ear, eye and glioma locations. Maximum deviations from the male analysis were 32.9 MHz for higher frequencies and 14.4 MHz for lower frequencies. They occur at the ear and intracranial positions in the model of the girl.

Inside the trunk and limbs, larger differences were found in some cases with respect analysis of the adult male. This can be attributed to the influence of the fat layer. The anatomical female model presents thicker fat areas in arm, chest and legs than the adult male and the children.

The most critical situation was found in the chest area. Figure 8 shows the same analysis performed for the male in the chest area (Figure 6(b)) but now using the female anatomical model. A maximum frequency shift towards higher frequencies of 72.9 MHz was observed when the antenna was located from 16 to 24 mm deep. For all the positions studied except the more superficial and the deepest locations (antenna inside muscle tissue), the impedance mismatch was over -10 dB. A maximum mismatch value of -28.5 dB was obtained for the female model. This detuning and impedance mismatch in the female chest region correspond with the maximum observed in the whole analysis in general and could be critical for the proper functioning of the antenna.

The influence of the fat tissue was not only observed in the chest, but also in other anatomical areas where the thickness of the fat layer varies from individual to individual. For instance, in the case of the

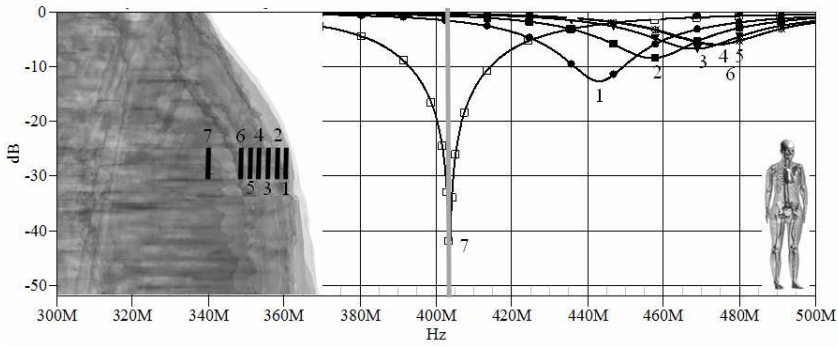

Figure 8. Simulated return losses for the antenna implanted inside the chest of the female anatomical computer model. The gray vertical line corresponds to the MISC reference frequency. The antenna was positioned 4 mm (1), 8 mm (2), 12 mm (3), 16 mm (4), 20 mm (5), 24 mm (6) and 40 mm (7) from the air-skin interface.

arm, large differences were observed between the models. Figure 9 shows the return loss when the antenna was located 15 mm from the skin-air interface. A small detuning of 7.4, 1.5 and 6.5 MHz for the adult male, girl and boy models, respectively, can be observed; and a large detuning of 42.3 MHz was observed for the adult female model.

Another interesting example is found in the abdominal region where different antenna detuning for children and adults can be clearly observed. Figure 10 illustrates the differences in detuning and impedance mismatch when the antenna was located 8 mm from the air-skin interface in the four models.

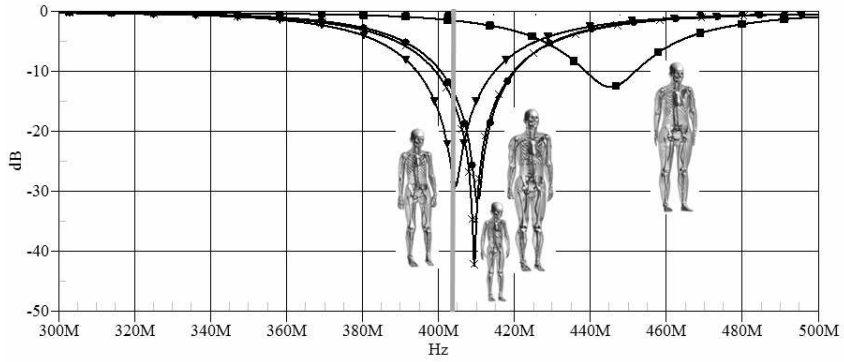

Figure 9. Simulated return losses for the antenna implanted inside the arm for the four anatomical computer models. The gray vertical line corresponds to the MISC reference frequency. The antenna was located 15 mm from the skin-air interface.

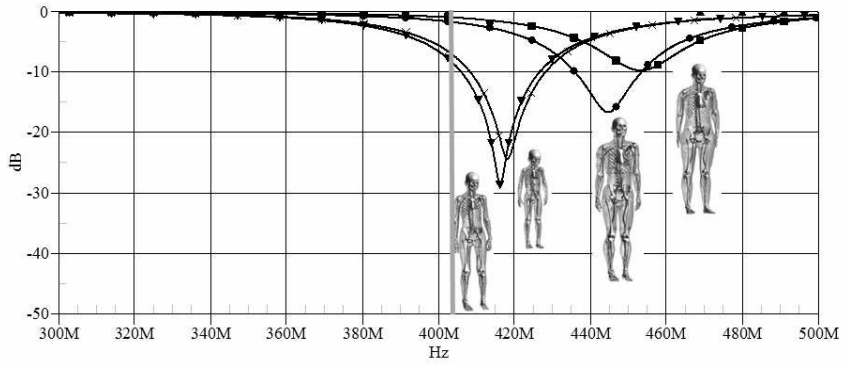

Figure 10. Simulated return losses for the antenna implanted inside the abdomen for the four anatomical computer models. The gray vertical line corresponds to the MISC reference frequency. The antenna was located 8 mm from the skin-air interface.

When the antenna was located inside the organs, the maximum deviation from the results for the male model was 2.8 MHz. In general, maximum deviations were around 2.5% (10 MHz). In general, the children showed less detuning for most of the locations studied than those obtained for the adults.

4. SUMMARY AND CONCLUSIONS

The detuning and impedance mismatch of antennas that were implanted in a simulated human body are presented. The study was carried out using electromagnetic modeling based on the finite-difference time-domain method. Four high-resolution anatomical models from the Virtual Family dataset were used. The implanted antennas operated in the MISC band. Thirty different locations were analyzed in head, trunk and limbs. The results are relevant to the design of implantable antennas. They indicate the bandwidth enhancement and initial tuning necessary for correct functioning.

Taking the 403 MHz MISC frequency as the reference, inside the head maximum frequency shifts towards higher frequencies of 45.5 MHz, and towards lower frequencies of 20.9 MHz were obtained. A maximum detuning bandwidth of 66.5 MHz was derived. Although mean values for head tissues were used to design the antenna, the frequency shift was observed not to occur symmetrically around 403 MHz. This means that due to anatomical distribution of tissues the frequency shift is mainly towards higher frequencies. The maximum mismatch deviation observed from the reference was about 10.1 dB. For all the cases studied, the resonance return losses remained below -10 dB. Some differences between the four anatomical models were derived with maximum deviations of 14 MHz for a single location.

Results from inside the trunk and limbs vary considerably depending on the antenna location. Besides the kidney and stomach, for the rest of the cases studied the antenna was always detuned towards higher frequencies. Detuning results below 390 MHz were never observed. This should lead to initial tuning of antennas to lower frequencies in order to compensate for this effect.

The most important detuning and impedance mismatch were found for subcutaneous locations and in areas where a thick fat layer is present. The strong influence of the thickness of the fat layer in the different areas was illustrated. Taking into account the anatomical computer models considered in the study, the most critical area was found to be the chest. Maximum detuning of 47.1 MHz for the male case and up to 73 MHz for the female analysis were observed. Impedance mismatch of over -10 dB was found for the most critical

cases in the female analysis, for the male analysis the resonant return losses always remained below −10 dB.

Inside the arm, abdomen and leg, large differences were also found between the different models due to the fat layer thickness. Notwithstanding, the detuning was lower than that found in the chest area and the resonance return losses remained below −10 dB.

Designing the antenna to have a resonant frequency of 403 MHz in a single tissue cannot guarantee that the antenna is going to work properly when inserted into different locations inside a high-resolution human body model or a real body. Bandwidth enhancement for implantable antennas may be a critical parameter to consider when the device has to be located in some specific areas. From our analysis, the frequency shift was observed not to occur symmetrically around 403 MHz, but shifted to higher frequencies. Accordingly, the antenna design should be centered at lower frequencies. Moreover, in order to compensate for frequency deviations, a minimum mean bandwidth of at least 70 MHz would be required.

ACKNOWLEDGMENT

This work was supported by the Spanish Ministry of Science and Innovation, project TEC2010-21484. The authors would like to thank M. Miñana from Schmid & Partner Engineering AG for her helpful advice with the software and especially during the process of gridding the anatomical models.

REFERENCES

1. Receveur, R. A. M., F. W. Lindemans, and N. F. de Rooij, "Microsystem technologies for implantable applications," *J. Micromech. Microeng.*, Vol. 17, 50–80, 2007.
2. Furse, C. M., "Biomedical telemetry: Today's opportunities and challenges," *IEEE Workshop on Antenna Technology Small Antennas and Novel Metamaterials*, Santa Monica, California, USA, Mar. 2009.
3. Soontornpipit, P., C. M. Furse, and Y. C. Chung, "Design of implantable microstrip antennas for communication with medical implants," *IEEE Transactions on Microwave Theory and Techniques*, Vol. 52, No. 8, 1944–1951, 2004.
4. Johnson, J., "Statistical analysis of detuning effects for implantable microstrip antennas," Ph.D. Thesis, University of Utah, 2007.

5. Kim, J. and Y. Rahmat-Samii, "Implanted antennas inside a human body: Simulations, designs, and characterizations," *IEEE Transactions on Microwave Theory and Techniques*, Vol. 52, No. 8, 1934–1943, 2004.
6. Rahmat-Samii, Y. and J. Kim, *Implanted Antennas in Medical Wireless Communications*, Morgan & Claypool Publishers, 2006.
7. Kim, J. and Y. Rahmat-Sammii, "Planar inverted-F antennas on implantable medical devices: Meandered type versus spiral type," *Microwave and Optical Technology Letters*, Vol. 48, No. 3, 567–572, 2006.
8. Lee, C. M., T. C. Yo, C. H. Luo, C. H. Tu, and Y.-Z. Juang, "Compact broadband stacked implantable antenna for biotelemetry with medical devices," *Electronics Letters*, Vol. 43, No. 12, 2007.
9. Lee, C. M., T. C. Yo, F. J. Huang, and C. H. Luo, "Dual-resonant P-shape with double L-strips PIFA for implantable biotelemetry," *Electronics Letters*, Vol. 44, No. 14, 2008.
10. Liu, W. C., F. M. Yeh, and M. Ghavami, "Minituarized implantable broadband antenna for biotelemetry communication," *Microwave and Optical Technology Letters*, Vol. 50, No. 9, 2407–2409, 2008.
11. Yilmaz, T., T. Karacolak, and E. Topsakal, "Characterization and testing of a skin mimicking material for implantable antennas operating at ISM Band," *IEEE Antennas and Wireless Propagation Letters*, Vol. 7, 418–420, 2008.
12. Karacolak, T., A. Z. Hood, and E. Topsakal, "Design of a dual-band implantable antenna and development of skin mimicking gels for continuous glucose monitoring," *IEEE Transactions on Microwave Theory and Techniques*, Vol. 56, No. 4, 1001–1008, 2008.
13. Karacolak, T., R. Cooper, J. Butler, S. Fisher, and E. Topsakal, "In vivo verification of implantable antennas using rats as model animals," *IEEE Antennas and Wireless Propagation Letters*, Vol. 9, 334–337, 2010.
14. Liu, W. C., S. H. Chen, and C. M. Wu, "Bandwidth enhancement and size reduction of an implantable PIFA antenna for biotelemetry devices," *Microwave and Optical Technology Letters*, Vol. 51, No. 3, 755–757, 2009.
15. Lee, C. M., T. C. Yo, F. J. Huang, and C. H. Luo, "Bandwidth enhancement of planar inverted-F antenna for implantable biotelemetry," *Microwave and Optical Technology Letters*, Vol. 51, No. 3, 749–752, 2009.

16. Vidal, N. and J. M. Lopez-Villegas, "Changes in electromagnetic field absorption in the presence of subcutaneous implanted devices: Minimizing increases in absorption," *IEEE Transactions on Electromagnetic Compatibility*, Vol. 52, No. 3, 545–555, 2010.
17. Gemio, J., J. Parrón, and J. Soler, "Human body effects on implantable antennas for ISM bands applications: Models comparison and propagation losses study," *Progress In Electromagnetics Research*, Vol. 110, 437–452, 2010.
18. Tan, K. B., X. An, F. F. Fan, and C. H. Liang, "Design of wideband microstrip printed monopole antenna with defected ground plane," *Journal of Electromagnetic Waves and Applications*, Vol. 24, No. 2–3, 169–178, 2010.
19. Kasabegoudar, V. G., "Low profile suspended microstrip antennas for wideband applications," *Journal of Electromagnetic Waves and Applications*, Vol. 25, No. 13, 1795–1806, 2011.
20. Christ, A., W. Kainz, E. G. Hahn, K. Honegger, M. Zefferer, E. Neufeld, W. Rascher, R. Janka, W. Bautz, J. Chen, B. Kiefer, P. Schmitt, H. P. Hollenbach, J. Shen, M. Oberle, D. Szczerba, A. Kam, J. W. Guag, and N. Kuster, "The virtual family-development of surface-based anatomical models of two adults and two children for dosimetric simulations," *Phys. Med. Biol.*, Vol. 55, 23–38, 2010.
21. "FCC guidelines for evaluating the environmental effects of radio frequency radiation," FCC, Washington, DC, 1996.
22. "Medical Implant Communications Service (MICS) federal register," *Rules and Regulations*, Vol. 64, No. 240, 69926–69934, 1999.
23. Neihart, N. M. and R. R. Harrison, "Micropower circuits for bidirectional wireless telemetry in neural recording applications," *IEEE Transactions on Biomedical Engineering*, Vol. 50, No, 11, 1950–1959, 2005.
24. Chow, E. Y., A. L. Chlebowski, and P. P. Irazoqui, "A miniature-implantable RF-wireless active glaucoma intraocular pressure monitor," *IEEE Transactions on Biomedical Circuits and Systems*, Vol. 4, No. 6, 340–349, 2010.
25. Chow, E. Y., A. L. Chlebowski, S. Chakraborty, W. J. Chappell, and P. P. Irazoqui, "Fully wireless implantable cardiovascular pressure monitor integrated with a medical stent," *IEEE Transactions on Biomedical Engineering*, Vol. 57, No. 6, 1487–1496, 2010.
26. Gao, Y., Y. Zheng, S. Diao, W. D. Toh, C. W. Ang, M. Je, and C. H. Heng, "Low-power ultrawideband wireless telemetry

transceiver for medical sensor applications," *IEEE Transactions on Biomedical Engineering*, Vol. 58, No. 3, 768–772, 2010.

27. Crescini, D., E. Sardini, and M. Serpelloni, "Design and test of an autonomous sensor for force measurements in human knee implants," *Sensors and Actuators*, Vol. 166, 1–8, 2011.
28. Noroozi, Z. and F. Hojjat-Kashani, "Three-dimensional FDTD analysis of the dual-band implantable antenna for continuous glucose monitoring," *Progress In Electromagnetics Research Letters*, Vol. 28, 9–21, 2012.
29. Parise, M., "On the use of cloverleaf coils to induce therapeutic heating in tissues," *Journal of Electromagnetic Waves and Applications*, Vol. 25, No. 11–12, 1667–1677, 2011.
30. Zhang, M. and A. Alden, "Calculation of whole-body SAR from a 100 mhz dipole antenna," *Progress In Electromagnetics Research*, Vol. 119, 133–153, 2011.
31. O'Halloran, M., M. Glavin, and E. Jones, "Rotating antenna microwave imaging system for breast cancer detection," *Progress In Electromagnetics Research*, Vol. 107, 203–217, 2010.
32. Yee, K. S., "Numerical solution of initial boundary value problems involving Maxwell's equations in isotropic media," *IEEE Trans. Antennas Propag.*, Vol. 14, No. 3, 302–307, 1966.
33. Sullivan, D. M., D. T. Borupa, and O. P. Gandhi, "Use of the finite-difference time-domain method in calculating EM absorption in human tissues," *IEEE Transactions on Biomedical Engineering*, Vol. 34, No. 2, 148–157, 1987.
34. SEMCAD X by SPEAG, www.semcad.com⟨http://www.semcad.-com⟩.
35. "Evaluating compliance with FCC guidelines for human exposure to radiofrequency electromagnetic fields," FCC, Washington, DC, 2001.
36. Smetana, W., B. Balluch, G. Stangl, E. Gaubitzer, M. Edetsberger, and G. Köhler, "A multi-sensor biological monitoring module built up in LTCC-technology," *Microelectronic Engineering*, Vol. 84, 1240–1243, 2007.
37. Bembnowicza, P., M. Małodobra, W. Kubicki, P. Szczepan Ska, A. Gorecka-Drzazga, J. Dziuban, A. Jonkisz, A. Karpiewskab, T. Dobosz, and L. Golonka, "Preliminary studies on LTCC based PCR microreactor," *Sensors and Actuators*, Vol. 150, 715–721, 2010.